Journal of Guidance, Control, and Dynamics, Vol. 41, No. 3, 2018, pp. 734–740. doi: https://doi.org/10.2514/1.G003169

Electric Sail Thrust Model from a Geometrical Perspective

Mingying Huo,* Giovanni Mengali† and Alessandro A. Quarta‡

(∗) *Department of Aerospace Engineering, Harbin Institute of Technology, Harbin 150006, China*

(†, ‡) *Department of Civil and Industrial Engineering, University of Pisa, I-56122 Pisa, Italy*

Nomenclature

A, B, C	=	auxiliary variables, see Eq. (12)
$\boldsymbol{a}$	=	propulsive acceleration vector (with $a = \|\boldsymbol{a}\|$), [mm/s^2]
a_c	=	characteristic acceleration, [mm/s^2]
b_i	=	cone angle curve-fit coefficient
c_i	=	dimensionless acceleration curve-fit coefficient
$\mathrm{d}s$	=	tether unit length, [km]
$\boldsymbol{F}$	=	thrust vector, [N]
$\hat{\boldsymbol{i}}_B$	=	unit vector of axis x_B
$\hat{\boldsymbol{j}}_B$	=	unit vector of axis y_B
$\hat{\boldsymbol{k}}_B$	=	unit vector of axis z_B
J	=	functional, [mm/s^2]
L	=	tether length, [km]
m	=	spacecraft total mass, [kg]
m_p	=	solar wind proton mass, [kg]
N	=	number of tethers
n	=	local solar wind number density, [cm^{-3}]
$\hat{\boldsymbol{n}}$	=	unit vector normal to the sail nominal plane
O	=	spacecraft center-of-mass, origin of $\mathcal{T}_B$
$\boldsymbol{r}$	=	Sun-spacecraft vector (with $r = \|\boldsymbol{r}\|$), [au]
$\boldsymbol{s}$	=	tether root-tip vector, [km]
$\mathcal{T}_B$	=	body reference frame
$\hat{\boldsymbol{t}}$	=	transverse unit vector
$\boldsymbol{u}$	=	solar wind velocity, [km/s]
V_k	=	k-th tether voltage, [kV]
V_w	=	solar wind electric potential, [kV]
x_B, y_B, z_B	=	axes of $\mathcal{T}_B$
α	=	cone angle, [deg]
α_n	=	pitch angle, [deg]
α_p	=	angle between $\hat{\boldsymbol{p}}$ and $\hat{\boldsymbol{r}}$, [deg]
α_r	=	polar angle of $\hat{\boldsymbol{r}}$, [deg]
δ_r	=	azimuthal angle of $\hat{\boldsymbol{r}}$, [deg]
ϵ_0	=	vacuum permittivity, [F/m]
τ	=	switching parameter
γ	=	dimensionless propulsive acceleration
$\sigma_\oplus$	=	tether maximum thrust magnitude per unit length, [N/m]
ζ	=	tether angular position, [deg]

Subscripts

0	=	initial, reference value
k	=	k-th tether
$\perp_k$	=	perpendicular to the k-th tether
r	=	radial
t	=	transverse
max	=	maximum
$\oplus$	=	Earth

Superscripts

$\star$	=	optimal
$\wedge$	=	unit vector
$\sim$	=	dimensionless

*Research assistant, huomingying123@gmail.com.

†Professor, g.mengali@ing.unipi.it. Senior Member AIAA.

‡Associate Professor, a.quarta@ing.unipi.it. Associate Fellow AIAA (**corresponding author**).

Introduction

The Electric Solar Wind Sail (E-sail) is a propellantless propulsion system concept that consists of thin centrifugally stretched tethers, charged by an onboard electron gun. The interaction of the artificial electric field generated by the tethers with the solar wind deflects the proton flow and generates a propulsive thrust. In the last years, much efforts have been dedicated to estimate the E-sail propulsive acceleration for mission analysis purposes, as is thoroughly discussed in Ref. [1].

In all of the available mathematical models [2–5] the E-sail thrust vector is written as a function of the Sun-spacecraft distance and the sail attitude, the latter being the angle between the direction of the local solar wind and the normal to the E-sail nominal plane. The accuracy and complexity of the available mathematical models vary depending on several factors, including the different plasmadynamic simulations and/or the inclusion of the curvature effect of the generic loaded tether.

The aim of this Note is to propose a compact vectorial description of the E-sail propulsive acceleration that takes into account the thrust contribution generated by any single tether. The obtained results may be translated into an elegant geometrical interpretation, which is particularly effective for optimal control law design.

Thrust Vector Analytical Model

Consider an E-sail that consists of $N \geq 2$ tethers, each one of length L, which are centrifugally stretched by the spacecraft spin and radially displaced from the vehicle main body, see Fig. 1(a). All tethers are assumed to belong to the same plane, referred to as sail nominal plane, orthogonal to the spacecraft spin axis.

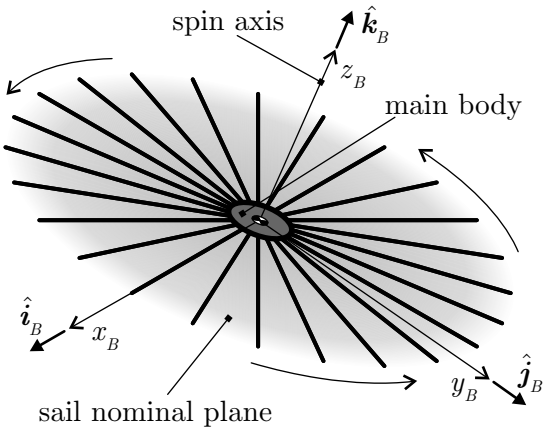

a) E-sail sketch.

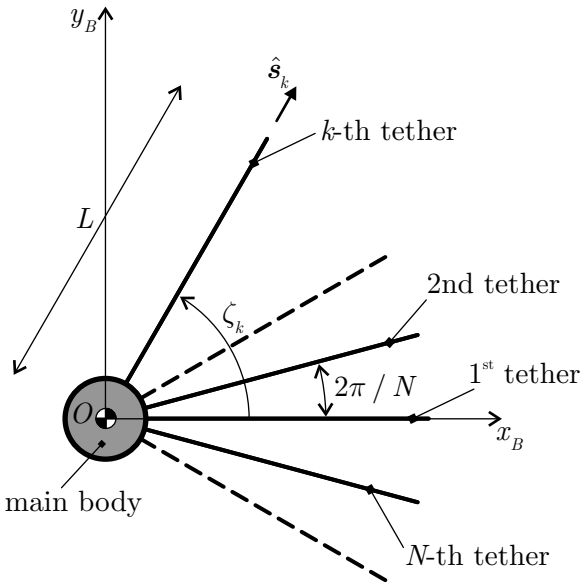

b) Tethers position in $\mathcal{T}_B(O; x_B, y_B, z_B)$.

Figure 1 E-sail conceptual scheme and body-axis reference frame.

To identify the position of the generic k-th tether (with $k = 1, 2, \ldots, N$), introduce a body-axis reference frame $\mathcal{T}_B(O; x_B, y_B, z_B)$, with origin O at the spacecraft center-of-mass and unit vectors $\hat{\boldsymbol{i}}_B$, $\hat{\boldsymbol{j}}_B$, and $\hat{\boldsymbol{k}}_B$, see Fig. 1(b). The plane (x_B, y_B) coincides with the sail nominal plane, x_B is aligned with the first tether (corresponding to $k = 1$), and $\hat{\boldsymbol{k}}_B$ coincides with the spacecraft spin velocity unit vector. Also, let $\hat{\boldsymbol{s}}_k$ be the unit vector aligned with the k-th tether and directed from its root to the tip. Assuming all tethers to be the same angle apart from each other (equal to $2\,\pi/N$ rad), the components of $\hat{\boldsymbol{s}}_k$ in the body-axis reference frame $\mathcal{T}_B$ are

$$[\hat{\boldsymbol{s}}_k]_{\mathcal{T}_B} = [\cos\zeta_k \quad \sin\zeta_k \quad 0]^{\mathrm{T}} \qquad \text{with} \qquad \zeta_k \triangleq \frac{2\,\pi(k-1)}{N} \tag{1}$$

where ζ_k is the angle between the direction of $\hat{\boldsymbol{\imath}}_B$ and that of $\hat{\boldsymbol{s}}_k$, measured counterclockwise from the x_B axis, see Fig. 1(b).

According to Refs. [3, 5, 6], when the Sun-spacecraft distance is on the order of 1 au, the force $\mathrm{d}\boldsymbol{F}$ per unit length $\mathrm{d}s$ generated by the k-th tether can be written as

$$\frac{\mathrm{d}\boldsymbol{F}}{\mathrm{d}s} = 0.18 \, \max\left(0, \, V_k - V_w\right) \sqrt{\epsilon_0 \, m_p \, n} \, \boldsymbol{u}_{\perp_k} \tag{2}$$

where V_k is the k-th tether voltage (on the order of $20-40\,\mathrm{kV}$), V_w is the electric potential corresponding to the kinetic energy of the solar wind ions (with a typical value of about $1\,\mathrm{kV}$), ϵ_0 is the vacuum permittivity, m_p is the solar wind ion (proton) mass, n is the local solar wind number density, and $\boldsymbol{u}_{\perp_k}$ is the component of the solar wind velocity $\boldsymbol{u}$ perpendicular to the k-tether direction. Assuming the solar wind to propagate radially from the Sun, the vectors $\boldsymbol{u}$ and $\boldsymbol{u}_{\perp_k}$ can be written as

$$\boldsymbol{u} = u \, \hat{\boldsymbol{r}} \tag{3}$$

$$\boldsymbol{u}_{\perp_k} = u \, (\hat{\boldsymbol{s}}_k \times \hat{\boldsymbol{r}}) \times \hat{\boldsymbol{s}}_k \equiv u \, [\hat{\boldsymbol{r}} - (\hat{\boldsymbol{s}}_k \cdot \hat{\boldsymbol{r}}) \, \hat{\boldsymbol{s}}_k] \tag{4}$$

where u is the solar wind flow speed (about $400\,\mathrm{km/s}$), and $\hat{\boldsymbol{r}}$ is the Sun-spacecraft unit vector, see Fig 2.

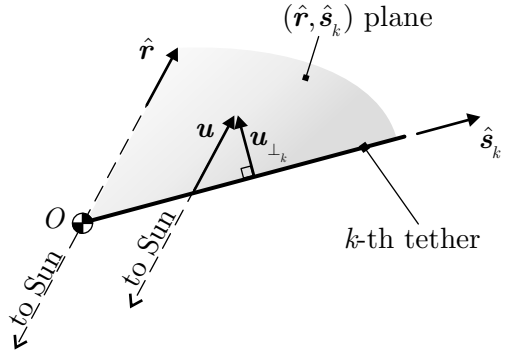

Figure 2 Components of solar wind velocity $\boldsymbol{u}$.

Recall that the local solar wind number density n is proportional to the inverse square distance from the Sun, i.e. $n = n_\oplus \, (r_\oplus/r)^2$ where $n_\oplus$ is the solar wind number density at $r = r_\oplus \triangleq 1\,\mathrm{au}$. Therefore, substituting Eq. (4) into Eq. (2), the force per unit length becomes

$$\frac{\mathrm{d}\boldsymbol{F}}{\mathrm{d}s} = \sigma_{\oplus_k} \left(\frac{r_\oplus}{r}\right) [\hat{\boldsymbol{r}} - (\hat{\boldsymbol{s}}_k \cdot \hat{\boldsymbol{r}}) \, \hat{\boldsymbol{s}}_k] \tag{5}$$

where

$$\sigma_{\oplus_k} \triangleq 0.18 \, \max\left(0, \, V_k - V_w\right) u \sqrt{\epsilon_0 \, m_p \, n_\oplus} \tag{6}$$

represents the maximum modulus of the specific force $\|\mathrm{d}\boldsymbol{F}/\mathrm{d}s\|$ given by the k-th tether at a Sun-spacecraft distance $r = r_\oplus$. Besides Eq. (2), other analytical models of the thrust force have been proposed for positively biased tethers, see e.g. Ref. [7]. The differences between the available models are however confined to the expression of $\sigma_{\oplus_k}$ and, therefore, the structure of Eq. (5) remains unchanged.

Since $\mathrm{d}\boldsymbol{F}/\mathrm{d}s$ is nearly constant along the tether, the total force $\boldsymbol{F}_k$ provided by the k-th tether of length L is

$$\boldsymbol{F}_k = L \, \sigma_{\oplus_k} \left(\frac{r_\oplus}{r}\right) [\hat{\boldsymbol{r}} - (\hat{\boldsymbol{s}}_k \cdot \hat{\boldsymbol{r}}) \, \hat{\boldsymbol{s}}_k] \tag{7}$$

Note that $\sigma_{\oplus_k}$ is a function of the tether voltage V_k, which may be slightly changed in any tether using a suitable potential control [3,5]. As a result, $\sigma_{\oplus_k}$ may not be the same for all tethers, see Eq. (6), and the general expression for the E-sail total thrust $\boldsymbol{F}$ is

$$\boldsymbol{F} = \tau \sum_{k=1}^{N} \boldsymbol{F}_k \equiv \tau \, L \left(\frac{r_\oplus}{r}\right) \hat{\boldsymbol{r}} \sum_{k=1}^{N} \sigma_{\oplus_k} - \tau \, L \left(\frac{r_\oplus}{r}\right) \sum_{k=1}^{N} \sigma_{\oplus_k} \, (\hat{\boldsymbol{s}}_k \cdot \hat{\boldsymbol{r}}) \, \hat{\boldsymbol{s}}_k \tag{8}$$

where $\boldsymbol{F}_k$ is given by Eq. (7). The dimensionless parameter $\tau \in \{0, \, 1\}$ is introduced in Eq. (8) to model the fact that the E-sail thrust can be turned off ($\tau = 0$) at any time by simply switching off the onboard electron gun.

An interesting form of the E-sail propulsive acceleration vector $\boldsymbol{a} = \boldsymbol{F}/m$, where m is the total spacecraft mass, is obtained when all of the tethers have the same voltage $V_k = V_0$ and, therefore, the same maximum modulus of specific force $\sigma_{\oplus_k}$. In that case, substituting $\sigma_{\oplus_k} = \sigma_\oplus$ into Eq. (8), the propulsive acceleration vector becomes

$$\boldsymbol{a} = \frac{\tau \, N \, L}{m} \, \sigma_\oplus \left(\frac{r_\oplus}{r}\right) \hat{\boldsymbol{r}} - \frac{\tau \, L}{m} \, \sigma_\oplus \left(\frac{r_\oplus}{r}\right) \sum_{k=1}^{N} (\hat{\boldsymbol{s}}_k \cdot \hat{\boldsymbol{r}}) \, \hat{\boldsymbol{s}}_k \tag{9}$$

Note that both Eqs. (8) and (9) neglect the sheath interference between tethers, which depends on several parameters, such as the voltage and the number of tethers.

The components of $\hat{\boldsymbol{r}}$ are now written in the body-axis reference frame $\mathcal{T}_B$ as a function of angles $\alpha_r \in [0, \, \pi]\,\mathrm{rad}$ and $\delta_r \in [0, \, 2\,\pi]\,\mathrm{rad}$, see Fig. 3, as

$$[\hat{\boldsymbol{r}}]_{\mathcal{T}_B} = [\sin\alpha_r \cos\delta_r \quad \sin\alpha_r \sin\delta_r \quad \cos\alpha_r]^{\mathrm{T}} \tag{10}$$

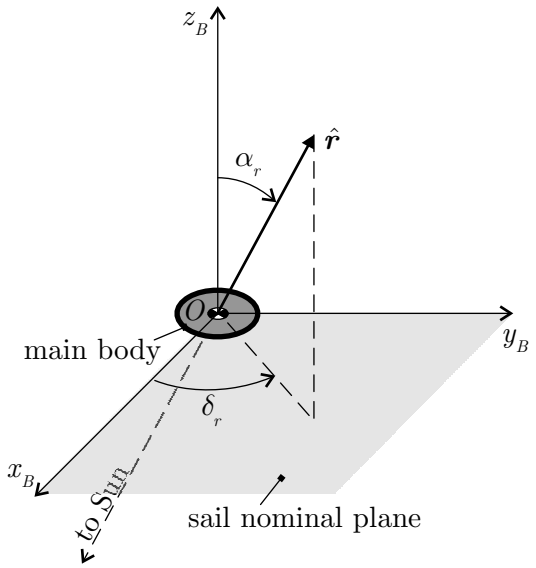

Figure 3 Components of the Sun-spacecraft position unit vector $\hat{\boldsymbol{r}}$.

Accordingly, the summation on the right-hand side of Eq. (9) becomes

$$\sum_{k=1}^{N} (\hat{\boldsymbol{s}}_k \cdot \hat{\boldsymbol{r}})\ \hat{\boldsymbol{s}}_k = \sin\alpha_r \left[(A\,\cos\delta_r + B\,\sin\delta_r)\,\hat{\boldsymbol{i}}_B + (B\,\cos\delta_r + C\,\sin\delta_r)\,\hat{\boldsymbol{j}}_B \right] \tag{11}$$

where

$$A \triangleq \sum_{k=1}^{N} \cos^2\zeta_k \quad , \quad B \triangleq \sum_{k=1}^{N} \cos\zeta_k\,\sin\zeta_k \quad , \quad C \triangleq \sum_{k=1}^{N} \sin^2\zeta_k \tag{12}$$

with ζ_k given by Eq. (1). It can be shown, see Appendix, that

$$A \equiv C = N/2 \qquad , \qquad B = 0 \tag{13}$$

Recalling Eq. (10), the summation in Eq. (11) reduces to

$$\sum_{k=1}^{N} (\hat{\boldsymbol{s}}_k \cdot \hat{\boldsymbol{r}})\ \hat{\boldsymbol{s}}_k = \frac{N}{2}\,\sin\alpha_r \left(\cos\delta_r\,\hat{\boldsymbol{i}}_B + \sin\delta_r\,\hat{\boldsymbol{j}}_B \right) \equiv \frac{N}{2} \left[\hat{\boldsymbol{r}} - \left(\hat{\boldsymbol{r}} \cdot \hat{\boldsymbol{k}}_B \right) \hat{\boldsymbol{k}}_B \right] \tag{14}$$

Substituting this last relation into Eq. (9), the spacecraft propulsive acceleration vector becomes

$$\boldsymbol{a} = \frac{\tau\,N\,L\,\sigma_\oplus}{2\,m} \left(\frac{r_\oplus}{r} \right) \left[\hat{\boldsymbol{r}} + \left(\hat{\boldsymbol{r}} \cdot \hat{\boldsymbol{k}}_B \right) \hat{\boldsymbol{k}}_B \right] \tag{15}$$

Note that $\left(\hat{\boldsymbol{r}} \cdot \hat{\boldsymbol{k}}_B \right) \hat{\boldsymbol{k}}_B \equiv (\hat{\boldsymbol{r}} \cdot \hat{\boldsymbol{n}})\ \hat{\boldsymbol{n}}$ with $\hat{\boldsymbol{r}} \cdot \hat{\boldsymbol{n}} \geq 0$, where $\hat{\boldsymbol{n}}$ is the unit vector normal to the sail nominal plane in the direction opposite to the Sun. A more compact expression of $\boldsymbol{a}$ may be obtained using the concept of spacecraft characteristic acceleration a_c, that is, the maximum modulus of the propulsive acceleration at a distance $r = r_\oplus$ from the Sun. Since $\|\boldsymbol{a}\|$ is maximum for a purely radial propulsive acceleration (that is, when $\hat{\boldsymbol{r}} = \hat{\boldsymbol{k}}_B$), from Eq. (15) the characteristic acceleration can be written as a function of $\sigma_\oplus$ as

$$a_c = \frac{N\,L\,\sigma_\oplus}{m} \tag{16}$$

Substituting Eq. (16) into Eq. (15), the final expression of the E-sail propulsive acceleration $\boldsymbol{a}$ becomes

$$\boldsymbol{a} = \tau\,\frac{a_c}{2} \left(\frac{r_\oplus}{r} \right) \left[\hat{\boldsymbol{r}} + (\hat{\boldsymbol{r}} \cdot \hat{\boldsymbol{n}})\ \hat{\boldsymbol{n}} \right] \tag{17}$$

In the general case when $\hat{\boldsymbol{n}} \neq \hat{\boldsymbol{r}}$ and $\tau = 1$, $\boldsymbol{a}$ belongs to the plane spanned by $(\hat{\boldsymbol{r}}, \hat{\boldsymbol{n}})$ and its direction is between $\hat{\boldsymbol{n}}$ and $\hat{\boldsymbol{r}}$, see Fig. 4. Furthermore, the propulsive acceleration modulus can be written as a function of the sail pitch angle $\alpha_n \triangleq \arccos(\hat{\boldsymbol{r}} \cdot \hat{\boldsymbol{n}}) \in [0,\, \pi/2]$ rad, that is, the angle between $\hat{\boldsymbol{n}}$ and $\hat{\boldsymbol{r}}$, as

$$a \triangleq \|\boldsymbol{a}\| = \tau\,\frac{a_c}{2} \left(\frac{r_\oplus}{r} \right) \sqrt{1 + 3\,\cos^2\alpha_n} \tag{18}$$

The pitch angle α_n is related to the more common sail cone angle $\alpha \in [0,\, \pi/2]$ rad, defined as the angle between $\hat{\boldsymbol{r}}$ and $\hat{\boldsymbol{a}}$, see Fig. 4. In fact, taking the scalar product of both sides of Eq. (17) by $\hat{\boldsymbol{r}}$, and substituting Eq. (18) into the resulting relation, it is found that

$$\alpha = \arccos\left(\frac{\boldsymbol{a} \cdot \hat{\boldsymbol{r}}}{a} \right) = \arccos\left(\frac{1 + \cos^2\alpha_n}{\sqrt{1 + 3\,\cos^2\alpha_n}} \right) \tag{19}$$

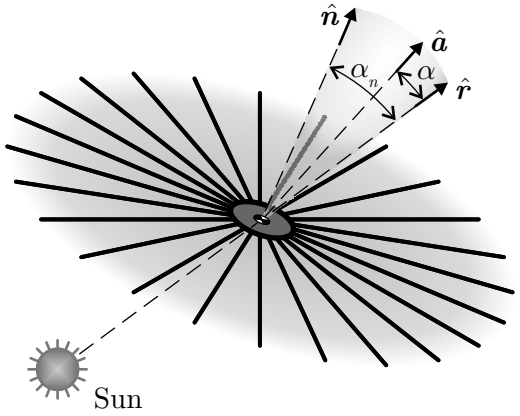

Figure 4 Pitch (α_n) and cone (α) angle.

Equation (19) states that $\alpha \leq \alpha_n/2$, that is, the direction of the propulsive acceleration is closer to $\hat{\boldsymbol{r}}$ than to $\hat{\boldsymbol{n}}$. In particular, when the sail nominal plane is orthogonal to the radial direction ($\alpha_n = \alpha = 0$), Eq. (17) reduces to

$$\boldsymbol{a} = \tau\, a_c \left(\frac{r_\oplus}{r}\right) \hat{\boldsymbol{r}} \tag{20}$$

which is the classical expression used to study the performance of a Sun-facing E-sail in an interplanetary mission scenario [8,9]. For small values of the pitch angle, that is, when $\alpha_n \leq 20\,\mathrm{deg}$, a good approximation of the cone angle is $\alpha \simeq \alpha_n/2$, which is in accordance with the simplified model used to characterize the thrust vector [2]. The latter point is clearly highlighted in Fig. 5, where the dimensionless propulsive acceleration modulus $a/(a_c\, r_\oplus/r)$ and the sail cone angle α are drawn as a function of the sail pitch angle α_n, see Eqs. (18)-(19). Note that $a_c\, r_\oplus/r$ is the local maximum value of a obtained with $\alpha_n = 0$ and $\tau = 1$.

The maximum modulus of the cone angle $\alpha_{\max}$ and the corresponding value of the sail pitch angle $\alpha_n(\alpha_{\max})$ are obtained by enforcing the necessary condition $\partial\alpha/\partial\alpha_n = 0$ in Eq. (19). The result is

$$\alpha_{\max} = \arcsin\left(1/3\right)\mathrm{rad} \simeq 19.5\,\mathrm{deg} \quad , \quad \alpha_n(\alpha_{\max}) = \arccos\left(1/\sqrt{3}\right)\mathrm{rad} \simeq 35.3\,\mathrm{deg} \tag{21}$$

Geometrical Interpretation

In the general case when $\hat{\boldsymbol{r}} \neq \hat{\boldsymbol{n}}$ and $\tau = 1$, there exists an interesting graphical representation of the E-sail propulsive acceleration vector. To that end, assuming $\alpha_n \neq 0$, introduce the transverse unit vector $\hat{\boldsymbol{t}} \triangleq [(\hat{\boldsymbol{r}} \times \hat{\boldsymbol{n}}) \times \hat{\boldsymbol{r}}]/\sin\alpha_n$. From the vector triple product rule

$$\hat{\boldsymbol{t}} = \frac{\hat{\boldsymbol{n}}}{\sin\alpha_n} - \frac{\hat{\boldsymbol{r}}}{\tan\alpha_n} \tag{22}$$

Substituting Eq. (22) into Eq. (17), the propulsive acceleration vector can be rewritten in terms of radial ($\boldsymbol{a}_r$) and transverse ($\boldsymbol{a}_t$) components as

$$\boldsymbol{a} = \boldsymbol{a}_r + \boldsymbol{a}_t \tag{23}$$

where

$$\boldsymbol{a}_r \triangleq \tau\, \frac{a_c}{4} \left(\frac{r_\oplus}{r}\right) \left[3 + \cos\left(2\,\alpha_n\right)\right] \hat{\boldsymbol{r}} \tag{24}$$

$$\boldsymbol{a}_t \triangleq \tau\, \frac{a_c}{4} \left(\frac{r_\oplus}{r}\right) \sin\left(2\,\alpha_n\right) \hat{\boldsymbol{t}} \tag{25}$$

In particular, from Eq. (25), the maximum modulus of the transverse propulsive acceleration is reached at a pitch angle $\alpha_n = \pi/4\,\mathrm{rad}$, that is, when the cone angle is $\alpha = \arccos\left(3/\sqrt{10}\right)\,\mathrm{rad} \simeq 18.5\,\mathrm{deg}$, see Eq. (19). The importance of this result is that the transverse component of the propulsive acceleration changes the specific orbital angular momentum vector $\boldsymbol{h}$ and, therefore, a sail pitch angle of $\alpha_n = \pi/4\,\mathrm{rad}$ maximizes the (local) variation of $\|\boldsymbol{h}\|$. The latter result is consistent with the analysis of Toivanen and Janhunen [5], who modelled the actual tether curvature using a simplified approach.

Notably, assuming $\tau = 1$, the E-sail propulsive acceleration vector may be described in graphical form using the polar plot of Fig. 6, in which

$$\widetilde{a}_r \triangleq \frac{\|\boldsymbol{a}_r\|}{a_c\, r_\oplus/r} = \frac{3 + \cos\left(2\,\alpha_n\right)}{4} \tag{26}$$

$$\widetilde{a}_t \triangleq \frac{\|\boldsymbol{a}_t\|}{a_c\, r_\oplus/r} = \frac{\sin\left(2\,\alpha_n\right)}{4} \tag{27}$$

According to Fig. 6, the function $\widetilde{a}_r = \widetilde{a}_r(\widetilde{a}_t)$ describes a half-circle in the plane $(\widetilde{a}_t,\, \widetilde{a}_r)$, with radius $R = 1/4$ and center $C = (0,\, 3/4)$. Therefore, a vector from the axes' origin o to a generic point P on the half-circle represents (when $\tau = 1$) the dimensionless propulsive acceleration vector $\widetilde{\boldsymbol{a}} \triangleq \boldsymbol{a}/(a_c\, r_\oplus/r)$ whose cone angle α is equal to the angle between the ordinate axis and the oP segment, while the pitch angle α_n coincides with one-half the angle between the ordinate axis and the CP segment, see Fig. 6 and Eqs. (26)-(27).

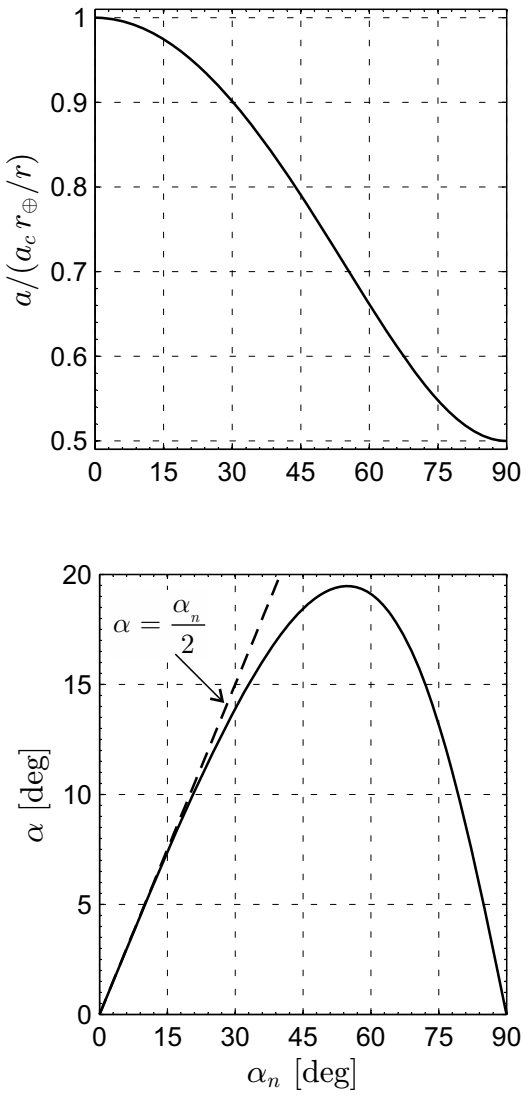

Figure 5 Dimensionless propulsive acceleration modulus and cone angle as a function of pitch angle (with $\tau = 1$).

Optimal Steering Law

The graphical representation of the propulsive acceleration vector of Fig. 6 is now used to find the value of the switching parameter τ and the optimal direction of $\hat{\boldsymbol{n}}$ that maximize the projection of $\boldsymbol{a}$ along a given unit vector $\hat{\boldsymbol{p}}$. This amounts to maximizing the scalar functional

$$J \triangleq \boldsymbol{a} \cdot \hat{\boldsymbol{p}} \tag{28}$$

The solution to this problem is important in the context of optimal heliocentric transfers, in particular when an indirect approach (based on the calculus of variations) is used to evaluate the minimum flight time to reach a prescribed target orbit. The steering law that maximizes J also provides the optimal thrust vector in a locally-optimal transfer, i.e. when the performance index to be maximized is a function of the (local) time variation of the spacecraft osculating orbit parameters.

In the special case when $\hat{\boldsymbol{p}} \equiv \hat{\boldsymbol{r}}$, the solution is simply a Sun-facing E-sail (i.e., $\hat{\boldsymbol{n}} = \hat{\boldsymbol{r}} \equiv \hat{\boldsymbol{p}}$) with $\tau = 1$. In that case, the propulsive acceleration modulus takes its maximum value, see Eq. (20), with $\tau = 1$. In the general case when $\hat{\boldsymbol{p}} \neq \hat{\boldsymbol{r}}$, the unit vector $\hat{\boldsymbol{n}}$ must belong to the plane spanned by $\hat{\boldsymbol{r}}$ and $\hat{\boldsymbol{p}}$, since a/τ depends on the sail attitude through the pitch angle only, see Eq. (18). Let $\alpha_p \triangleq \arccos(\hat{\boldsymbol{p}} \cdot \hat{\boldsymbol{r}}) \in [0,\, \pi]$ rad be the angle between $\hat{\boldsymbol{p}}$ and $\hat{\boldsymbol{r}}$. Recalling Eq. (17), the functional J becomes

$$J = \tau\, \frac{a_c}{2}\, \left(\frac{r_\oplus}{r}\right) [\cos\alpha_p + \cos\alpha_n\, \cos(\alpha_p - \alpha_n)] \tag{29}$$

Enforcing the necessary condition $\partial(J/\tau)/\partial\alpha_n = 0$, the last relation provides a compact expression for the optimal pitch angle $\alpha_n^\star$, that is

$$\alpha_n^\star = \alpha_p/2 \tag{30}$$

whereas Eq. (29) gives the maximum value of the ratio J/τ as a function of the angle α_p, viz.

$$\max(J/\tau) = \frac{a_c}{4}\, \left(\frac{r_\oplus}{r}\right)\, (1 + 3\, \cos\alpha_p) \tag{31}$$

In other terms, according to Eq. (30), the optimal direction of $\hat{\boldsymbol{n}}$ coincides with the bisector of the angle between $\hat{\boldsymbol{r}}$ and $\hat{\boldsymbol{p}}$.

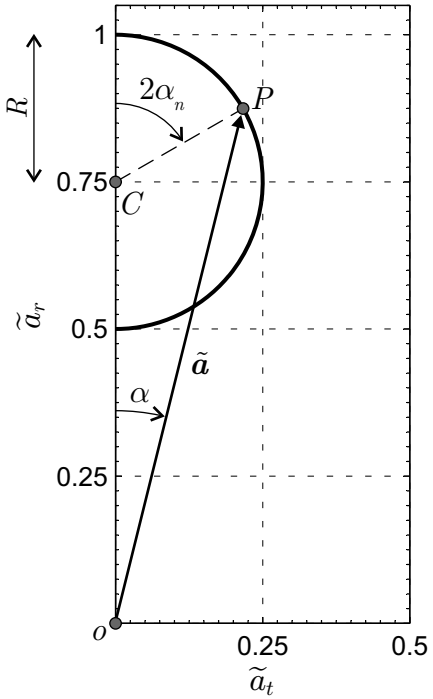

Figure 6 Polar plot of the dimensionless propulsive acceleration components (with $\tau = 1$).

The optimal value $\tau^\star$ can be found by observing that J is a linear function of τ, see Eq. (29). Therefore, the resulting bang-bang optimal control law is $\tau^\star = 1$ when $\max(J/\tau) \geq 0$, and $\tau^\star = 0$ when $\max(J/\tau) < 0$. In other terms, from Eq. (31)

$$\tau^\star = \frac{\operatorname{sign}(1 + 3\,\cos\alpha_p) + 1}{2} \equiv \frac{\operatorname{sign}(1 + 3\,\hat{\boldsymbol{p}}\cdot\hat{\boldsymbol{r}}) + 1}{2} \tag{32}$$

where $\operatorname{sign}(\cdot)$ is the signum function.

The results of Eqs. (30) and (32) may also be recovered with a geometric approach, using the polar plot shown in Fig. 7. In fact, the maximum of the projection of $\boldsymbol{a}/\tau$ along $\hat{\boldsymbol{p}}$ is found by looking for the PH segment that is both tangent to the half-circle (which describes the locus of points where the tip of vector $\widetilde{\boldsymbol{a}}$ lies) and orthogonal to $\hat{\boldsymbol{p}}$. Since CP and oH are parallel segments, it follows that $\alpha_p = 2\,\alpha_n^\star$. Note that, taking into account the expression of $\alpha_{\max}$ given by Eq. (21), the condition $\tau^\star = 0$ described by Eq. (32) is obtained when the direction of $\hat{\boldsymbol{p}}$ lies in the shaded area of Fig. 7.

From Eq. (30), the optimal sail orientation defined by the unit vector $\hat{\boldsymbol{n}}^\star \triangleq \hat{\boldsymbol{n}}(\alpha_n^\star)$ is

$$\hat{\boldsymbol{n}}^\star = \frac{\cos(\alpha_p/2)}{1 + \cos\alpha_p}\,(\hat{\boldsymbol{r}} + \hat{\boldsymbol{p}}) \tag{33}$$

When Eqs. (32) and (33) are substituted into Eq. (17), the optimal propulsive acceleration $\boldsymbol{a}^\star = \boldsymbol{a}(\alpha_n^\star, \tau^\star)$ may be written as a function of $\hat{\boldsymbol{p}}$, $\boldsymbol{r}$ and a_c as

$$\boldsymbol{a}^\star = \frac{a_c}{8}\left(\frac{r_\oplus}{r}\right)(3\,\hat{\boldsymbol{r}} + \hat{\boldsymbol{p}})\,[\operatorname{sign}(1 + 3\,\hat{\boldsymbol{p}}\cdot\hat{\boldsymbol{r}}) + 1] \tag{34}$$

In the special case when $\alpha_p = 0$, that is $\hat{\boldsymbol{p}} = \hat{\boldsymbol{r}}$, Eq. (33) simply states that $\hat{\boldsymbol{n}}^\star = \hat{\boldsymbol{r}}$, while Eq. (34) reduces to Eq. (20) with $\tau = 1$.

Comparison with the Literature Results

The previous thrust vector model provides an elegant analytical proof of the numerical model proposed by Yamaguchi and Yamakawa [4, 10] in which the cone angle α and the propulsive acceleration modulus a are both functions of the sail pitch angle α_n.

In particular, according to Refs. [4,10], when the thruster is on ($\tau = 1$), the sail cone angle depends on the sail pitch angle through a sixth-order polynomial equation that fits the numerical results, viz.

$$\alpha = b_6\,\alpha_n^6 + b_5\,\alpha_n^5 + b_4\,\alpha_n^4 + b_3\,\alpha_n^3 + b_2\,\alpha_n^2 + b_1\,\alpha_n + b_0 \tag{35}$$

where the coefficients b_i, with $i = 1, 2, \ldots, 6$ are summarized in Tab. 1. The model of Yamaguchi and Yamakawa [4, 10] also provides the following expression for the propulsive acceleration modulus

$$a = a_c\,\tau\left(\frac{r_\oplus}{r}\right)\gamma \tag{36}$$

where γ is a sort of dimensionless propulsive acceleration. The value of γ depends, again, on the sail pitch angle α_n through a best-fit sixth-order polynomial equation in the form

$$\gamma = c_6\,\alpha_n^6 + c_5\,\alpha_n^5 + c_4\,\alpha_n^4 + c_3\,\alpha_n^3 + c_2\,\alpha_n^2 + c_1\,\alpha_n + c_0 \tag{37}$$

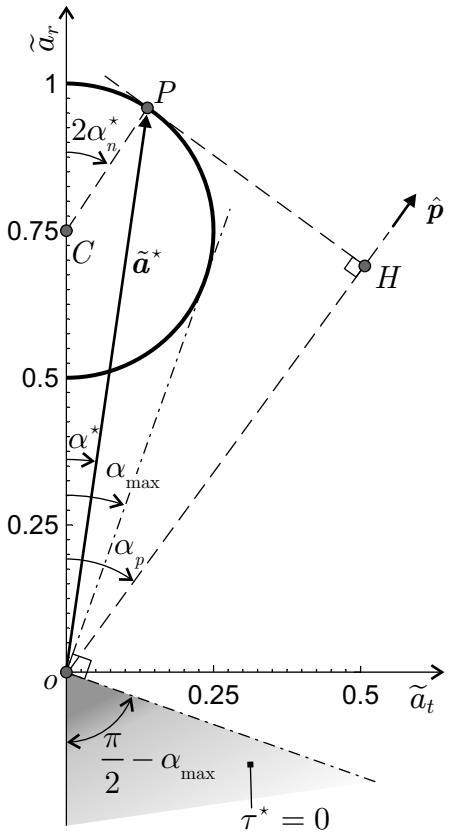

Figure 7 Graphical approach to find the optimal steering law.

i	0	1	2	3	4	5	6
b_i	0	4.853×10^{-1}	3.652×10^{-3}	-2.661×10^{-4}	6.322×10^{-6}	-8.295×10^{-8}	3.681×10^{-10}
c_i	1	6.904×10^{-5}	-1.271×10^{-4}	7.027×10^{-7}	-1.261×10^{-8}	1.943×10^{-10}	-5.896×10^{-13}

Table 1 Best-fit interpolation coefficients of thrust model (angles in degrees) by Yamaguchi and Yamakawa [4, 10]. Table adapted from Ref. [1].

whose coefficients c_i are collected in Tab. 1.

The results of Fig. 5 are in perfect agreement with the plot of the function $\alpha = \alpha(\alpha_n)$ in Eq. (35) with coefficients b_i taken from Tab. 1. Also, upon comparing Eq. (36) and Eq. (18), the dimensionless propulsive acceleration γ of Refs. [4, 10] can be written as a function of the sail pitch angle as

$$\gamma = \frac{\sqrt{1 + 3\,\cos^2\alpha_n}}{2} \tag{38}$$

The correctness of the last relation is confirmed by a plot of the polynomial function $\gamma = \gamma(\alpha_n)$ given by Eq. (37), which overlaps to the upper curve drawn in Fig. 5.

Starting from the model by Yamaguchi and Yamakawa [4, 10], Ref. [1] discusses the optimal control law using both an analytical and a graphical approach. In the latter case, the curve $\widetilde{a}_r = \widetilde{a}_r(\widetilde{a}_t)$ calculated with Eqs. (35) and (37) is approximated with a circle of radius $\rho \simeq 0.2523$ and center $C = (0,\, d)$ with $d \simeq 0.7477$. The resulting expressions for γ and α are [1]

$$\gamma = \sqrt{d^2 + \rho^2 + 2\,\rho\,d\,\cos(2\,\alpha_n)} \tag{39}$$

$$\alpha = \arctan\left(\frac{\rho\,\sin(2\,\alpha_n)}{d + \rho\,\cos(2\,\alpha_n)}\right) \tag{40}$$

Notably, these last two relations coincide with Eqs. (19) and (38) when $\rho = R = 1/4$ and $d = 3/4$, see Fig. 6. Moreover, the results obtained in Ref. [1] show that the optimal pitch angle is about one half of α_p, as is stated by Eq. (30), and the optimal switching parameter is zero when α_p is greater than a critical value of about 110 deg. In fact, according to Fig. 7 and Eq. (32), the critical value of α_p is $\arccos(-1/3) \equiv (\alpha_{\max} + \pi/2) \simeq 110\,\text{deg}$.

Finally, recalling that $\left(\hat{\boldsymbol{r}} \cdot \hat{\boldsymbol{k}}_B\right)\, \hat{\boldsymbol{k}}_B \equiv (\hat{\boldsymbol{r}} \cdot \hat{\boldsymbol{n}})\, \hat{\boldsymbol{n}}$ with $\hat{\boldsymbol{r}} \cdot \hat{\boldsymbol{n}} \geq 0$, the vectorial model of Eq. (17) gives the same result of Ref. [5] when the tethers are assumed to be straight. However, it is worth noting that the analysis of Toivanen and Janhunen [5] is based on the assumption of a continuous angular distribution of the tethers and, as such, on a sufficiently high number N of available tethers. The model of this Note, instead, can be applied to an arbitrary number of tethers with $N \geq 2$ and provides a vectorial relation that is very useful for a preliminary analysis of an orbital transfer.

Conclusions

The propulsive acceleration generated by an electric solar wind sail may be described in vectorial form as a function of the angle between the propagation direction of the solar wind and the spacecraft spin axis. The acceleration vector has a simple and effective geometrical interpretation that illustrates the relation existing between the sail pitch angle and the cone angle. Likewise, the optimal sail attitude for minimum time transfer trajectories can be easily visualized in graphical form.

The new results, which are very useful for preliminary mission analyses, have been compared to existing models obtained using numerical simulations. The limits of the new model are confined to the assumptions adopted, in particular to the fact that the tethers must be straight and all belonging to the same plane. A more refined analysis should account for the curvature of each tether due to the solar wind load and the tension due to the centrifugal force. The latter point requires a dynamical analysis of the tethers and a substantial complication of the mathematical model.

Appendix

Using standard trigonometric identities, the coefficients A, B and C of Eqs. (12) may be rewritten as

$$A = \sum_{\ell=0}^{N-1} \frac{1+\cos(2\,\zeta_\ell)}{2} \quad , \quad B = \sum_{\ell=0}^{N-1} \frac{1}{2}\,\sin(2\,\zeta_\ell) \quad , \quad C = \sum_{\ell=0}^{N-1} \frac{1-\cos(2\,\zeta_\ell)}{2} \tag{41}$$

where, from Eq. (1), $\zeta_\ell = 2\,\pi\,\ell/N$. The evaluation of the three coefficients reduces to calculating the two summations in $\cos(2\,\zeta_\ell)$ and $\sin(2\,\zeta_\ell)$. To that end, note that

$$\sum_{\ell=0}^{N-1} \cos(2\,\zeta_\ell) = \sum_{\ell=0}^{N-1} \frac{\mathrm{e}^{j\,2\zeta_\ell} + \mathrm{e}^{-j\,2\zeta_\ell}}{2} = \frac{1}{2}\sum_{\ell=0}^{N-1} \left[\mathrm{e}^{(j\,4\pi/N)}\right]^\ell + \frac{1}{2}\sum_{\ell=0}^{N-1} \left[\mathrm{e}^{(-j\,4\pi/N)}\right]^\ell \tag{42}$$

The last two summations in Eq. (42) are in the form of a geometric series. Recalling that

$$\sum_{\ell=0}^{N-1} x^\ell = \frac{1-x^N}{1-x} \tag{43}$$

where x is the common ratio of the series, Eq. (42) becomes

$$\sum_{\ell=0}^{N-1} \cos(2\,\zeta_\ell) = \frac{1}{2}\,\frac{1-\mathrm{e}^{j\,4\pi}}{1-\mathrm{e}^{j\,4\pi/N}} + \frac{1}{2}\,\frac{1-\mathrm{e}^{-j\,4\pi}}{1-\mathrm{e}^{-j\,4\pi/N}} = 0 \tag{44}$$

Likewise, using a similar approach, it can be verified that

$$\sum_{\ell=0}^{N-1} \sin(2\,\zeta_\ell) = 0 \tag{45}$$

The final result $A = C = N/2$ and $B = 0$, see Eq. (13), is immediately obtained by substituting Eqs. (44) and (45) into Eq. (41).

References

[1] Quarta, A. A. and Mengali, G., "Minimum-Time Trajectories of Electric Sail with Advanced Thrust Model," *Aerospace Science and Technology*, Vol. 55, August 2016, pp. 419–430. doi: 10.1016/j.ast.2016.06.020.

[2] Mengali, G., Quarta, A. A., and Janhunen, P., "Electric Sail Performance Analysis," *Journal of Spacecraft and Rockets*, Vol. 45, No. 1, January-February 2008, pp. 122–129. doi: 10.2514/1.31769.

[3] Toivanen, P. and Janhunen, P., "Spin Plane Control and Thrust Vectoring of Electric Solar Wind Sail," *Journal of Propulsion and Power*, Vol. 29, No. 1, January-February 2013, pp. 178–185. doi: 10.2514/1.B34330.

[4] Yamaguchi, K. and Yamakawa, H., "Study on Orbital Maneuvers for Electric Sail with On-Off Thrust Control," *Aerospace Technology Japan*, Vol. 12, 2013, pp. 79–88. doi: 10.2322/astj.12.79.

[5] Toivanen, P. and Janhunen, P., "Thrust Vectoring of an Electric Solar Wind Sail with a Realistic Sail Shape," *Acta Astronautica*, Vol. 131, 2017, pp. 145–151. doi: 10.1016/j.actaastro.2016.11.027.

[6] Janhunen, P., Toivanen, P. K., Polkko, J., Merikallio, S., Salminen, P., Haeggstrom, E., Seppanen, H., Kurppa, R., Ukkonen, J., Kiprich, S., Thornell, G., Kratz, H., Richter, L., Kromer, O., Rosta, R., Noorma, M., Envall, J., Latt, S., Mengali, G., Quarta, A. A., Koivisto, H., Tarvainen, O., Kalvas, T., Kauppinen, J., Nuottajarvi, A., and Obraztsov, A., "Electric Solar Wind Sail: Towards Test Missions," *Review of Scientific Instruments*, Vol. 81, No. 11, 2010, pp. 111301 (1–11). doi: 10.1063/1.3514548.

[7] Sanchez-Torres, A., "Propulsive Force in an Electric Solar Sail," *Contributions to Plasma Physics*, Vol. 54, No. 3, 2014, pp. 314–319. doi: 10.1002/ctpp.201410077.

[8] Mengali, G., Quarta, A. A., and Aliasi, G., "A Graphical Approach to Electric Sail Mission Design with Radial Thrust," *Acta Astronautica*, Vol. 82, No. 2, February 2013, pp. 197–208. doi: 10.1016/j.actaastro.2012.03.022.

[9] Quarta, A. A. and Mengali, G., "Analysis of Electric Sail Heliocentric Motion under Radial Thrust," *Journal of Guidance, Control and Dynamics*, Vol. 39, No. 6, June 2016, pp. 1431–1435. doi: 10.2514/1.G001632.

[10] Yamaguchi, K. and Yamakawa, H., "Electric Solar Wind Sail Kinetic Energy Impactor for Near Earth Asteroid Deflection Mission," *The Journal of the Astronautical Sciences*, Vol. 63, No. 1, March 2016, pp. 1–22. doi: 10.1007/s40295-015-0081-x.